International Journal of Minerals, Metallurgy and Materials
Volume 21, Number 10, October 2014, Page 1009
DOI: 10.1007/s12613-014-1002-x

Non-monotonic influence of a magnetic field on the electrochemical behavior of $Fe_{78}Si_9B_{13}$ glassy alloy in NaOH and NaCl solutions

Hong-di Zhang[1)], *Xiao-yu Li*[2)], *Jing Pang*[2)], *Li-juan Yin*[2)], *Hai-jian Ma*[1,3)], *Ying-jie Li*[1)], *Yan Liu*[1)], *and Wei-min Wang*[1)]

1) Key Laboratory for Liquid-Solid Structural Evolution and Processing of Materials (Ministry of Education), Shandong University, Jinan 250061, China
2) Qingdao Yunlu Energy Technology Co. Ltd., Qingdao 266109, China
3) School of Mechanical and Electrical Engineering, Weifang University, Weifang 261061, China
(Received: 12 March 2014; revised: 21 April 2014; accepted: 24 April 2014)

Abstract: The corrosion behavior and microstructure of $Fe_{78}Si_9B_{13}$ glassy alloy in NaOH and NaCl solutions under a 0.02-T magnetic field were investigated through electrochemical testing and scanning electron microscopy (SEM). The current-density prepeak (PP) in the anodic polarization curves in low-concentration NaOH solutions (classified as type I) tends to disappear when the NaOH concentration is increased to 0.4 mol/L and the magnetic field is applied. Under the magnetic field, the height of the second current-density peak is increased in low-concentration NaOH solutions (type I) but decreased in high-concentration NaOH solutions (type II). The non-monotonic effect of the magnetic field was similarly observed in the case of polarization curves of samples measured in NaCl solutions. Ring-like corroded patterns and round pits are easily formed under the magnetic field in NaOH and NaCl solutions. These experimental results were discussed in terms of the magnetohydrodynamic (MHD) effect.

Keywords: amorphous alloys; electrochemical behavior; magnetic field; anodic polarization; micrographs

1. Introduction

Fe-based amorphous alloys, because of their special microstructure, exhibit interesting characteristics, such as excellent soft magnetic properties, high strength, and improved resistance to corrosion, which differ from the properties of their corresponding crystalline alloys [1–5]. In particular, $Fe_{78}Si_9B_{13}$ glassy alloy has been widely used in power transformers and electronic devices, which are always under the influence of a magnetic field. Many power transformers are installed outdoors and utilized for more than twenty years. Hence, the corrosion resistance of $Fe_{78}Si_9B_{13}$ glassy alloy under a magnetic field is a worthwhile topic of study.

Numerous investigations have revealed that the introduction of a magnetic field affects the corrosion behavior of Fe-based glassy alloys, and the literature contains some controversial views on this topic [6]. Electrochemical testing has been used to investigate the effect of magnetic fields on the corrosion properties of amorphous alloys, and the anodic polarization of these alloys can be divided into several stages, such as anodic dissolution, a mass transport range, and a passive range [7].

The mass transport rates of electrochemical reactions have been observed to closely depend on the magnetic field, which can be analyzed on the basis of the magnetohydrodynamic (MHD) theory [8]. Digital holography technology is also used in the investigation of the magnetic field effect of corrosion behavior in different solutions [9–13]. In recent years, the electrochemical behavior of iron in acidic solutions, alkali solutions, and aqueous solutions under a magnetic field with a fixed flux density or different flux densities has been widely discussed [14–17].

The theoretical implications and potential practical applications of the applied magnetic field to govern electrochemical behavior have been used in industry, such as to

Corresponding author: Wei-min Wang E-mail: weiminw@sdu.edu.cn

enhance mass transfer, improve electrodeposition quality, and control potential distribution and current [18–21]. However, to our knowledge, the literature contains few reports on the corrosion behavior of Fe-based glassy alloys in NaOH solutions with different concentrations or in the solutions with chloride ions under a magnetic field. Electrochemical investigations of Fe-based amorphous alloys in different environments are helpful in widening their potential applications in industry.

The aim of this study was to characterize the influence of a superimposed magnetic field on the corrosion behavior of $Fe_{78}Si_9B_{13}$ glassy alloy in different NaOH and NaCl solutions. Furthermore, the corroded surfaces of the glassy alloy were investigated after the application of a magnetic field. The experimental results were discussed in terms of the MHD effects.

2. Experimental

Glassy $Fe_{78}Si_9B_{13}$ ribbons were supplied by the National Amorphous Nanocrystalline Alloy Engineering Research Center of China. Evaluations of corrosion resistance were performed by electrochemical testing in a typical three-electrode system, consisting of a working electrode (a stationary specimen, labeled as WE), a platinum counter electrode (CE), and a reference electrode (RE). As evident from the schematic diagram in Fig. 1, the magnetic field was introduced via two ferrite magnets with the same size. The electrolytic cell was centered between the magnets, and the magnetic field intensity was 0.02 T. The electrolytes included NaOH and NaCl solutions with different concentrations. For electrochemical testing, the working side of all the glassy ribbons was the wheel side, whereas the other side was covered by epoxy resin. The size of specimen was 40 mm in length, 10 mm in width, and 35 μm in thickness. The ribbons were cleaned using an autocleaner for 30 min and then cleaned them with alcohol prior to electrochemical measurements. During the testing, the ribbons were immersed vertically in the electrolytes such that the magnetic induction lines passed vertically through the working side of the glassy ribbons. The potentiodynamic polarization curves were investigated using an LK 2005A advanced electrochemical workstation with a 5 mV/s scan rate. All the electrochemical measurements were performed at room temperature and repeated at least three times to ensure good reproducibility. The surface morphologies of the ribbons after polarization experiments were examined using scanning electron microscopy (SEM, Zeiss SUPRA 55).

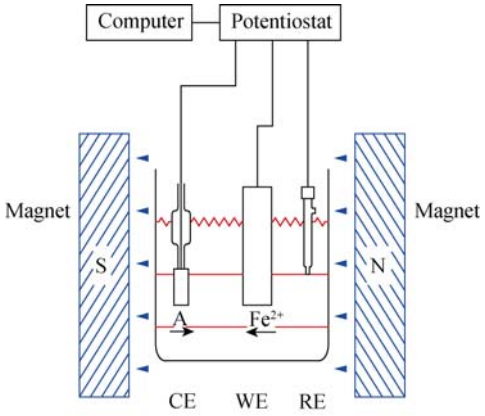

Fig. 1. Schematic of the apparatus employed for electrochemical testing.

3. Results

3.1. Anodic polarization curves of $Fe_{78}Si_9B_{13}$ glassy alloy in NaOH solutions

(1) In the absence of a magnetic field. The potentiodynamic polarization curves of $Fe_{78}Si_9B_{13}$ glassy alloy in 0.01–1 mol/L NaOH solutions in the presence or absence of a magnetic field are presented in Fig. 2. All of the anodic curves show an active-passive-transpassive process, which is similar to that reported in previous works [7,22]. In 0.01–0.2 mol/L NaOH solutions, earlier oxidation occurs at about −0.85 V and forms a current-density prepeak denoted by PP. With increasing potential E, the polarization curves show a first peak (P1) at E_{P1} and then a second peak (P2) at E_{P2}. Subsequently, the current density decreases to a plateau region range from the passive potential (E_{pass}) to the transpassive potential (E_{TP}), i.e., the passive zone. At the end of the polarization curve, the current density increases dramatically from E_{TP}.

In 0.4–1 mol/L NaOH solutions, the polarization curves show only two peaks (P1 and P2) before the passive region, and a current-density bump (BP) in the passive zone becomes increasingly apparent with increasing concentration. Notably, BP appears in the passive zone, which means the metastable passivation occurs during the process. In 0.4 mol/L NaOH solution, PP is much lower in intensity than P1 and can be neglected. BP is as high as P1 in 1 mol/L NaOH solution. Furthermore, the passive range becomes narrower with increasing NaOH concentration. On the basis of the variation of the current-density peaks with increasing NaOH concentration, the anodic polarization curves were categorized into types I and II for the curves in 0.01–0.2 mol/L and in 0.4–1 mol/L NaOH solutions, respectively.

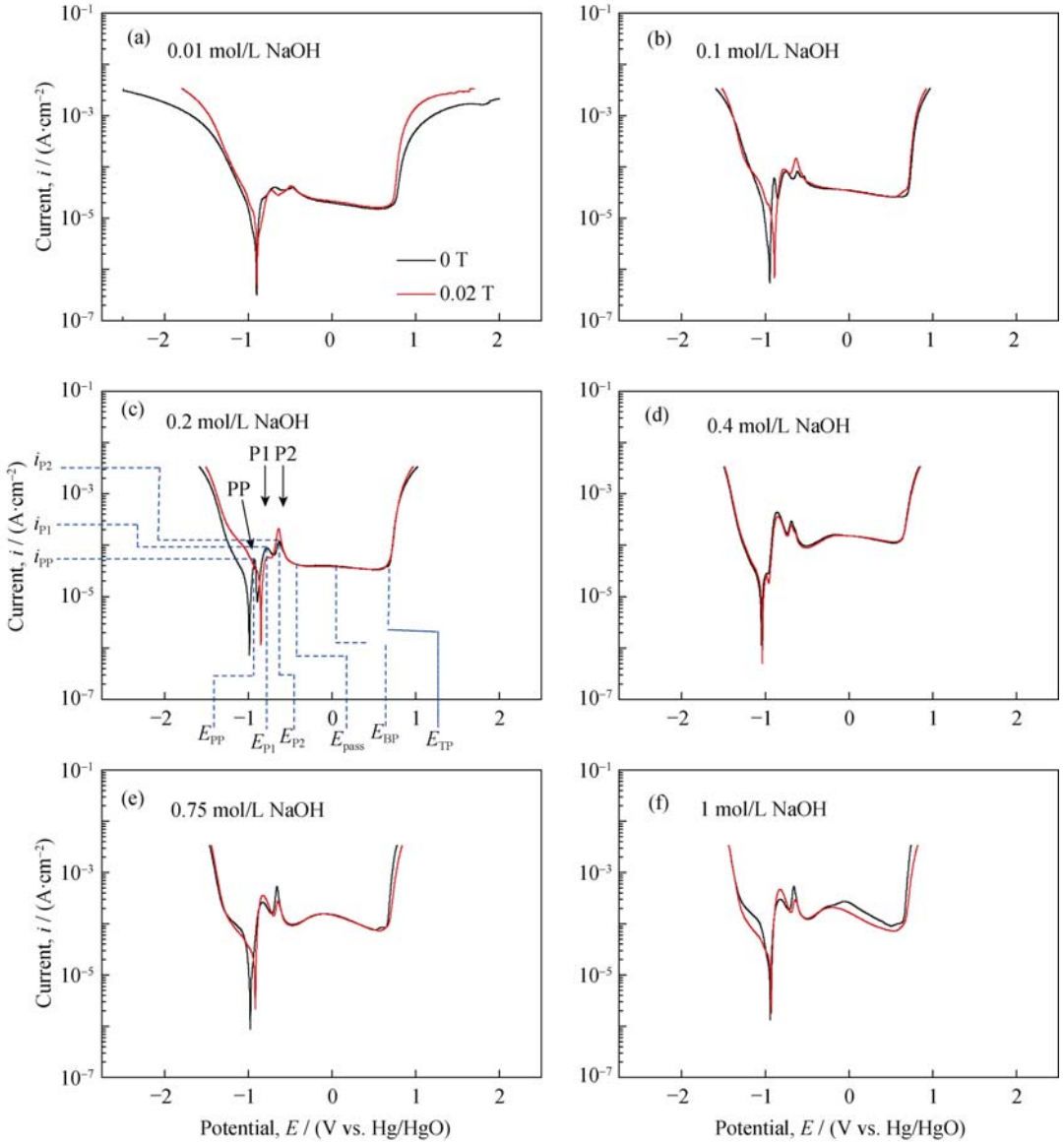

Fig. 2. Potentiodynamic polarization curves of $Fe_{78}Si_9B_{13}$ glassy alloy in NaOH solutions in the absence and presence of a 0.02-T magnetic field: (a) 0.01 mol/L NaOH; (b) 0.1 mol/L NaOH; (c) 0.2 mol/L NaOH; (d) 0.4 mol/L NaOH; (e) 0.75 mol/L NaOH; (f) 1 mol/L NaOH.

(2) In the presence of a magnetic field. The polarization curves of $Fe_{78}Si_9B_{13}$ glassy alloy under a 0.02-T magnetic field are also presented in Fig. 2. Under the magnetic field, the type I anodic polarization curves (in 0.01–0.2 mol/L NaOH solutions) exhibit only two current-density peaks before the passive region. Compared with the electrochemical reactions in the absence of the magnetic field, the corrosion potentials of the polarization curves under the magnetic field tend to shift to higher potentials. Under the magnetic field, the P1 in type II anodic polarization curves is much higher than that in type I curves.

Fig. 3 shows the characteristic potentials and current densities of $Fe_{78}Si_9B_{13}$ glassy alloy in NaOH solutions with and without the magnetic field; the potentials and current densities are deduced from Fig. 2. Here, the peak potentials E_{PP}, E_{P1}, and E_{P2} of type I curves decrease monotonically with increasing NaOH concentration. However, the potentials E_{P1} and E_{P2} of type II curves are almost unchanged, as shown in Fig. 3(a). In the passive polarization range, the passive potential (E_{pass}), the metastable potential (E_{BP}), and the transpassive potential (E_{TP}) of type I curves all decrease with increasing NaOH concentration, whereas these potentials of type II curves increase slightly, as shown in Fig. 3(b). In the investigated NaOH solutions, the characteristic cur-

rent density i_{P2} of samples with and without the magnetic field increases monotonically with increasing NaOH concentration. However, the increase rate of i_{P2} in type II curves is obviously lower than that in type I curves, as shown in Fig. 3(c). In addition, the change in i_{P2} after applying the magnetic field ($\Delta i_{P2}=i_{P2}(0.02\ T)-i_{P2}(0\ T)$) is positive for type I curves, but is negative for type II curves in Fig. 3(d).

(3) Microstructure of corroded glassy ribbons. Fig. 4 shows the microstructure of samples after electrochemical testing in 0.4 mol/L NaOH solution. Two regions are observed on the corroded alloy surface: a severely corroded region and a less-corroded region, i.e., a bared region (Rb) and a covered region (Rc), respectively, which are similar to the corroded surface of iron in H_2SO_4 solutions [23]. Some small white corroded particles are present in the covered region in the absence of the magnetic field, as shown in Figs. 4(a) and (b), whereas no such particles are formed under the magnetic field, resulting in a cleaner appearance in Figs. 4(c) and (d). Moreover, the pattern in bared region changes after the magnetic field is applied, resulting in a circular ring-like shape on the glassy ribbon surface.

3.2. Anodic polarization curves of $Fe_{78}Si_9B_{13}$ glassy alloy in NaCl solutions

(1) In the absence of a magnetic field. The anodic polarization curves of $Fe_{78}Si_9B_{13}$ glassy alloy in NaCl solutions are shown in Fig. 5. The electrochemical reaction in NaCl solutions is significantly different from that in NaOH solutions. The anodic polarization curves can be divided into two zones (Z1 and Z2) before the fierce pitting process, and one current-density peak is observed in each zone. In 0.05 mol/L NaCl solution (Fig. 5(a)), the current-density peaks in Z1 and Z2 zones range from −1.9 to −0.2 V and are followed by a pitting process instead of a passive region, which is similar to the results reported in previous works [24]. When the NaCl concentration is higher, the current-density peak in Z1 zone decreases in intensity (Figs. 5(b)–(d)). In Z2 zone, the anodic current density increases quickly with increasing potential; i.e., the current density in the middle of Z2 zone (i_{Z2}) increases with increasing NaCl concentration.

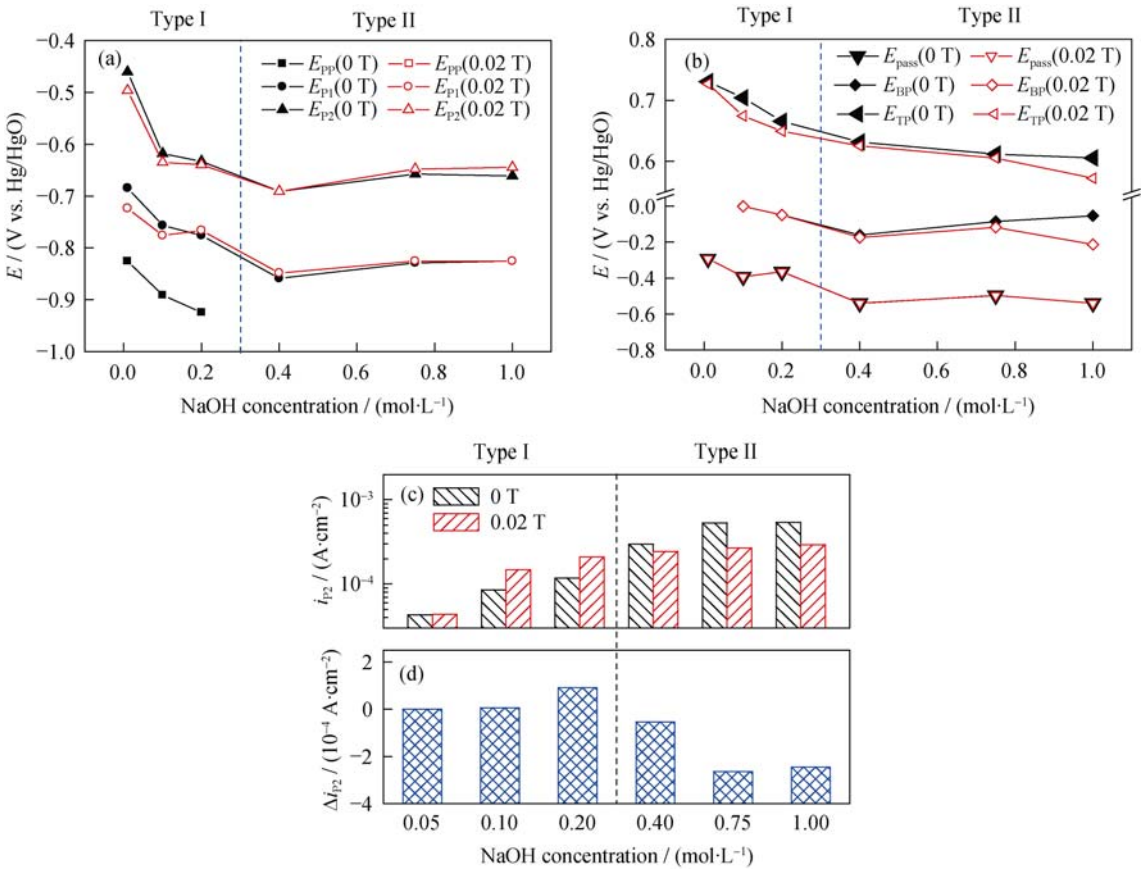

Fig. 3. Characteristic potentials and current densities in anodic polarization curves for $Fe_{78}Si_9B_{13}$ glassy alloy in x mol/L NaOH solutions (x = 0.01, 0.1, 0.2, 0.4, 0.75, and 1) in the absence and presence of a 0.02-T magnetic field: (a,b) characteristic potentials; (c,d) characteristic current densities.

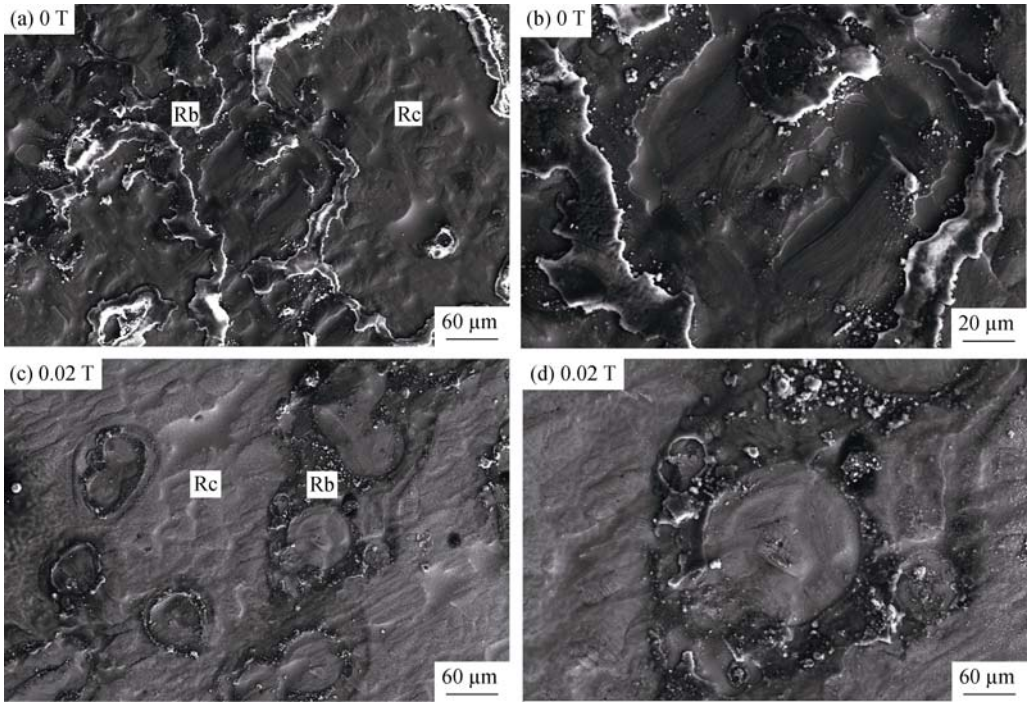

Fig. 4. Surface SEM micrographs of $Fe_{78}Si_9B_{13}$ glassy ribbons corroded in 0.4 mol/L NaOH solution in the absence ((a) and (b)) and presence ((c) and (d)) of a 0.02-T magnetic field.

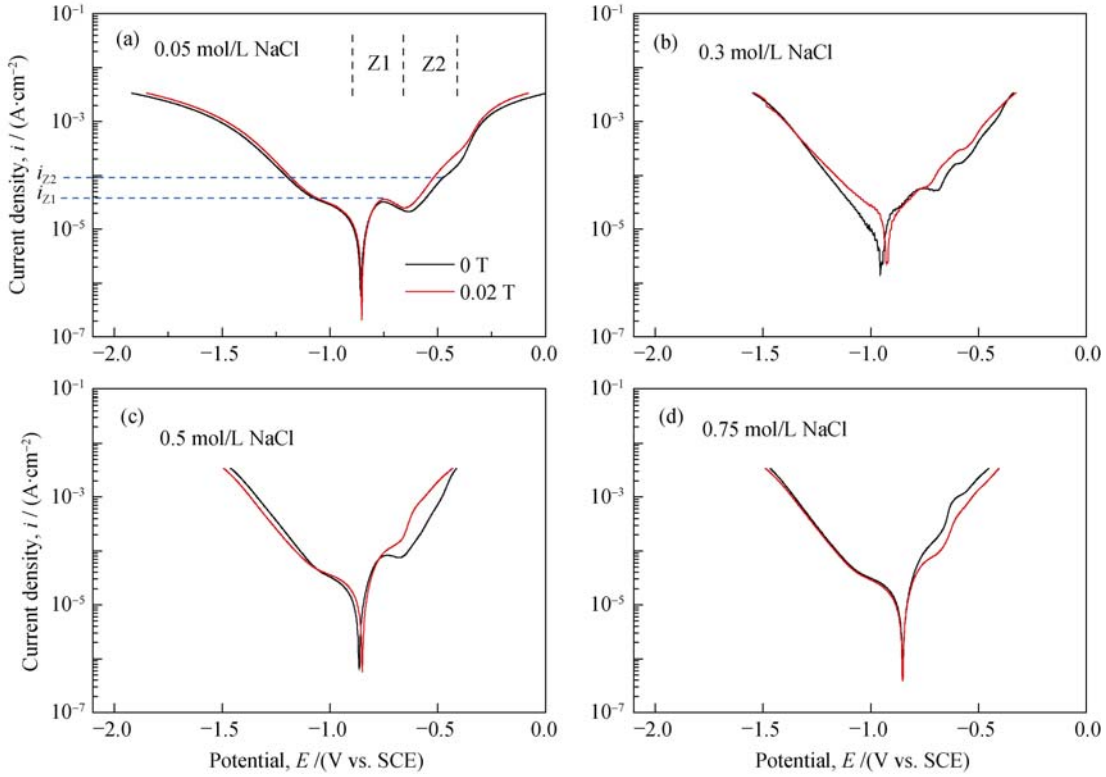

Fig. 5. Potentiodynamic polarization curves for $Fe_{78}Si_9B_{13}$ glassy alloy in x mol/L NaCl solutions in the absence and presence of a 0.02-T magnetic field: (a) x = 0.05; (b) x = 0.3; (c) x = 0.5; (d) x = 0.75.

(2) In the presence of a magnetic field. As shown in Fig. 5, the shape of the anodic polarization curves of $Fe_{78}Si_9B_{13}$ glassy alloy in NaCl solutions does not change under the applied magnetic field. In 0.05–0.5 mol/L NaCl solutions (Figs. 5(a)–(c)), the current density in the middle of Z1 zone (i_{Z1}) in the presence of a 0.02-T magnetic field is similar to

that in the absence of a magnetic field. In contrast, i_{Z2} under a 0.02-T magnetic field is obviously higher than that in the absence of the magnetic field. In 0.75 mol/L NaCl solution (Fig. 5(d)), however, the current density i_{Z2} under a 0.02-T magnetic field is less than that in the absence of the magnetic field. The current density i_{Z2} with and without the magnetic field and the change in current density $\Delta i_{Z2} = i_{Z2}(0.02\ \text{T}) - i_{Z2}(0\ \text{T})$ are shown in Fig. 6. The anodic polarization curves are categorized into two types: the type with a low NaCl concentration and the type with a high NaCl concentration, i.e., type I′ and type II′, similar to those in NaOH solutions. In the measured solutions, i_{Z2} in the absence of a 0.02-T magnetic field increases monotonically with increasing NaCl concentration, whereas i_{Z2} under a 0.02-T magnetic field first increases and then decreases. Δi_{Z2} in type I′ is positive, but is negative in type II′.

(3) Microstructure of the corroded glassy ribbons. The corrosion morphologies of the glassy ribbons after polarization in 0.05 mol/L NaCl solution without and with a 0.02-T magnetic field are shown in Fig. 7. In the absence of the magnetic field, numerous tubers as well as small pits appear on the sample surface, as shown in Fig. 7(a), and microcracks disperse on the surface of tubers, as shown in Fig. 7(b). The average diameter of pits is approximately 7 μm. In contrast, the number of pits on the sample surface polarized under a 0.02-T magnetic field, especially round-shaped pits, is greater than that of the sample polarized in the absence of the magnetic field, as shown in Fig. 7(c). Some cracks occur in the radial direction from the pit center, and white particles are densely distributed on the surface, resulting in a higher roughness of the matrix compared to that of the sample treated in the absence of the magnetic field, as shown in Fig. 7(d). The average diameter of pits increases to 11 μm under a 0.02-T magnetic field. In addition, the pit morphology is similar to that of the Cu–Zr metallic glasses in hydrochloric acid solutions [25]. Furthermore, the pit mouths exhibit layers on their rims, which gives a stepped appearance and results in the deep pits.

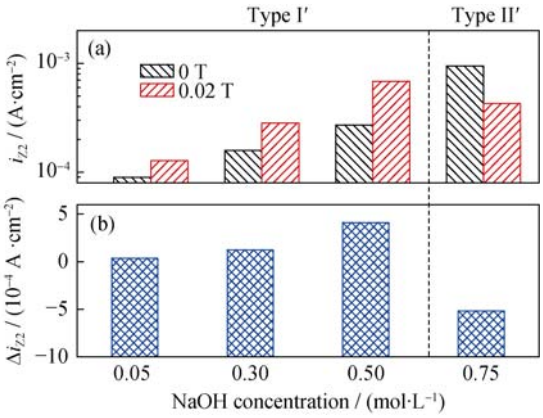

Fig. 6. Characteristic current density in anodic polarization curves for $Fe_{78}Si_9B_{13}$ glassy alloy in x mol/L NaCl (x = 0.05, 0.3, 0.5, 0.75) solutions in the presence and absence of a 0.02-T magnetic field: (a) i_{Z2}; (b) Δi_{Z2}.

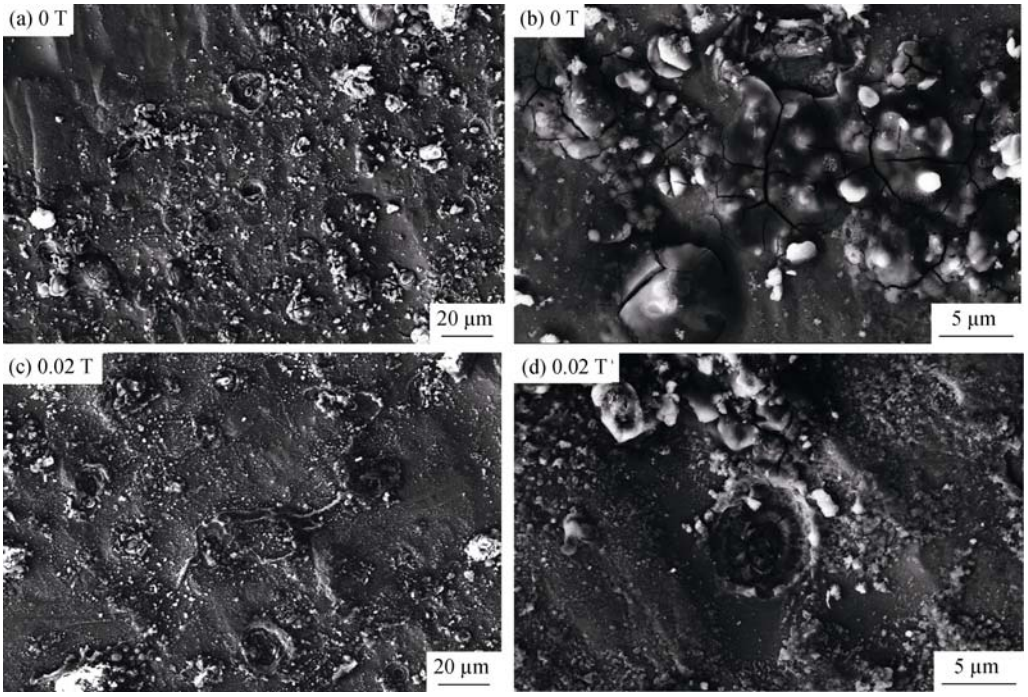

Fig. 7. SEM micrographs of $Fe_{78}Si_9B_{13}$ glassy alloy corroded in 0.05 mol/L NaCl solution in the absence (a,b) and presence (c,d) of a 0.02-T magnetic field.

4. Discussion

4.1. Anodic polarization behavior of $Fe_{78}Si_9B_{13}$ glassy alloy in NaOH solutions

According to the explanation of the active dissolution and passivation process of iron in alkaline solutions [22,26], the hydro-ligand MOH_{ads} (where M represents a metal) is the dominant product in the dissolution process at relatively low potentials [27]. Hence, the current-density prepeak (E_{PP}) at low potentials is associated with the formation of a low-valence oxide, which can be expressed as

$$Fe \rightleftharpoons Fe^{2+} + 2e^- \quad (1)$$

$$Fe + 2OH^- \rightleftharpoons Fe(OH)_2 + 2e^- \quad (2)$$

The secondary metabolite $Fe(OH)_2$ disperses on the glassy alloy surface in a porous state [28]. During the electrochemical testing, the low-valence oxides formed at low potentials undergo the further oxidation reaction [22]. Thus, the first current-density peak (E_{P1} in Fig. 2(c)) should be associated with the active adsorption of OH^- as the following equation:

$$3Fe(OH)_2 + 2OH^- \rightleftharpoons Fe_3O_4 + 4H_2O + 2e^- \quad (3)$$

The second current-density peak (E_{P2} in Fig. 2(c)) is associated with the further oxidation reactions, which can be expressed as

$$2Fe_3O_4 + 2OH^- \rightleftharpoons 3Fe_2O_3 + H_2O + 2e^- \quad (4)$$

$$Fe(OH)_2 + OH^- \rightleftharpoons Fe(OH)_3 + e^- \quad (5)$$

$$2Fe(OH)_3 \rightleftharpoons Fe_2O_3 + 3H_2O \quad (6)$$

Eqs. (3)–(6) are the reactions based on the secondary metabolites $Fe(OH)_2$, whereas the oxide Fe_xO_y is also scattered on the porous matrix. Notably, the formation of Fe_3O_4 at the base of $Fe(OH)_2$ is easier than the formation of Fe_2O_3. The Fe_3O_4 can be regarded as $FeO{\cdot}Fe_2O_3$ and the average valence of iron is +8/3, whereas the average valence of iron in Fe_2O_3 is +3. Furthermore, the standard electrode potentials of Fe/Fe^{2+} and Fe/Fe^{3+} at room temperature (approximately 25°C) are −0.440 and −0.036 V, respectively [29], suggesting that the oxidation reaction of Fe/Fe^{3+} requires more energy than that of Fe/Fe^{2+}. The aforementioned facts confirm that the first and second peaks in the polarization curves represent the generation of oxides Fe_3O_4 and Fe_2O_3, respectively.

Silicon in the sample also participates in the reaction in sodium hydroxide solutions, which can be written as follows [29]:

$$Si + 2NaOH + H_2O \rightleftharpoons Na_2SiO_3 + 2H_2 \quad (7)$$

The oxidation product Na_2SiO_3 usually exists in the form of $Na_2O{\cdot}nSiO_2$, which is known as water glass in industry. Na_2SiO_3 is easily dissolved in high-concentration NaOH solutions [29]. Hence, Eq. (7) only occurs in passive range and corresponds to the bump in polarization curves at approximately 0 V. The oxygen-evolution reaction may occur at sufficiently high anodic potentials (E_{TP}). This reaction can be written as

$$2H_2O \rightleftharpoons O_2 + 4H^+ + 4e^- \quad (8)$$

For type I curves, three current-density peaks appear before the passive zone; these peaks represent the generation of $Fe(OH)_2$, Fe_3O_4, and Fe_2O_3 films, respectively. However, only two current-density peaks appear in the type II curves. According to Fig. 2, the prepeak intensity decreases and the peak finally disappears with increasing NaOH concentration, indicating that the previous oxidation of $Fe(OH)_2$ results in its direct transformation into Fe_3O_4 in high-concentration NaOH solutions. These current-density peaks and their variations have been reported in previously published work [30].

The current density of anodic polarization for iron in alkali solutions (i_a) can be calculated by the following equation [22]:

$$i_a = \frac{i_{0,a}\exp\left[\frac{2.303(E-E_{e,a})}{b_a}\right] + i_{0,ff}\exp\left[\frac{2.303(E-E_{e,ff})}{b_{ff}}\right]}{1+\frac{Ci_{0,ff}\exp\left[\frac{2.303(E-E_{e,ff})}{b_{ff}}\right]}{\eta}} \quad (9)$$

where the subscripts a and ff represent the anodic dissolution and anodic film formation reactions, respectively; i_0, E_e, and b stand for the exchange current density, equilibrium potential, and Tafel slope for the anodic reactions, respectively; and C is the surface area of the formed film. The constant $\eta = \eta(T, \text{pH}, OH^-)$ as the surface-film dissolution rate is a function of temperature, pH value, and the concentration of film-forming ion OH^-. Here, the constant η increases with increasing OH^- concentration, which results in an increase in the anodic current density according to Eq. (9). Hence, as shown in Fig. 3(c), the current peak density i_{P2} increases with increasing OH^- concentration.

4.2. Anodic polarization behavior $Fe_{78}Si_9B_{13}$ glassy alloy in NaCl solutions

The anodic reactions of $Fe_{78}Si_9B_{13}$ glassy alloy in NaCl solutions (Fig. 5) are much more severe than those in NaOH solutions (Fig. 2). The polarization curves in NaCl solutions exhibit only two zones prior to the fierce pitting, indicating

the generation of Fe^{2+} and Fe^{3+} according to the Refs. [29,31]. According to Eq. (9), the constant $\eta = \eta(T, \text{pH}, OH^-)$ as the film dissolution rate can be transformed into $\eta' = \eta'(T, \text{pH}, Cl^-)$ in NaCl solutions, and the constant η increases with increasing concentration [22]. Hence, the current density i_{Z2} of the samples is expected to increase with increasing NaCl concentration (Fig. 6). The chloride ion is known to destroy the oxidation film, and further dissolution occurs at the destroyed surface [32], which results in the drastic increase in current density, i.e., the occurrence of pitting (Figs. 7(a)–(b)). Previous reports have demonstrated that the chloride ion can stimulate the pitting process of $Zr_{65}Al_{7.5}Ni_{10}Cu_{17.5}$ amorphous alloy in a phosphate buffered solution [33]. According to Figs. 3(c)–(d) and Fig. 6, the variation of current density i_{Z2} in NaCl solutions is similar to that of i_{P2} in NaOH solutions.

4.3. Effect of magnetic field on the anodic polarization of $Fe_{78}Si_9B_{13}$ glassy alloy

Previous research has been conducted on the effects of magnetic fields on the corrosion behavior of glassy alloys [23,34]. In general, the mass transport rate at the metal/solution interface is enhanced by the application of a magnetic field via the MHD effect. Two factors facilitate the movement of a charged particle in the boundary layer of electrode at a velocity of $\boldsymbol{V_0}$ under an applied magnetic field, the electric field force, $\boldsymbol{F_E}$, and the magnetic field force (MHD force), $\boldsymbol{F_{MHD}}$, which are defined as the following equation:

$$\boldsymbol{F} = \boldsymbol{F_E} + \boldsymbol{F_{MHD}} \quad (10)$$

$$\boldsymbol{F_E} = q\boldsymbol{E} \quad (11)$$

$$\boldsymbol{F_{MHD}} = \boldsymbol{J} \times \boldsymbol{B} \quad (12)$$

where $\boldsymbol{F}$ represents the total force, q the charge quantity of particle, $\boldsymbol{E}$ the electrical field intensity, $\boldsymbol{J}$ the current density, and $\boldsymbol{B}$ the magnetic field intensity.

The total movement velocity of a charged particle, $\boldsymbol{V_T}$, can be expressed by the vector sum.

$$\boldsymbol{V_T} = \boldsymbol{V_0} + \boldsymbol{V_{mag}} \quad (13)$$

where $\boldsymbol{V_{mag}}$ is the MHD velocity. According to Fleming's rule and Eq. (12), $\boldsymbol{V_{mag}}$ has a circular direction [35].

(1) In NaOH solutions. As shown in Fig. 2, the prepeak PP, which indicates the formation of $Fe(OH)_2$, decreases in intensity and then disappears with increasing NaOH concentration. In addition, the PP in type I curves are repressed under an applied magnetic field. This phenomenon can be explained by the MHD effect [36–37] as the following, under a magnetic field, the enhanced mass transport action promotes the movement of OH^- from the electrolyte to the alloy surface and then increases the local OH^- concentration. Thus, the initial $Fe(OH)_2$ film is transformed into a Fe_3O_4 film by the extra OH^- under a 0.02-T magnetic field (Fig. 2), which is similar to the phenomenon reported by Lu *et al.* [22]. Moreover, the current density (i_a^*) under the magnetic field (B) can be expressed through Eq. (9) by the modified constant $\eta^* = \eta^*(T, \text{pH}, OH^-, B)$ as the film dissolution rate. In low-concentration solutions, $\eta^* = \eta^*(T, \text{pH}, OH^-, B) > \eta = \eta(T, \text{pH}, OH^-)$. As a consequence, $i_{P2}(0.02\ \text{T}) > i_a(0\ \text{T})$ in type I curves.

However, in the case of type II curves, the increase rate of the second current-density peak i_{P2} decreases with increasing NaOH concentration in the presence of the magnetic field, resulting in a non-monotonic variation of the current-density difference Δi_{P2} with increasing NaOH concentration. In general, the electrochemical current density is expected to be proportional to the reactant concentration [38]. In nitrobenzene (NB) solutions, the viscosity of a solution will increase when the NB concentration is greater than 0.1 mol/L, although the increase in current will tend to deviate from the expected value with increasing NB concentration. Meanwhile, the NB ions are electrogenerated at a maximum rate in the solution containing 2 mol/L NB, and the magnetic field effect shows a maximum at a NB concentration of 2 mol/L [39–41]. Hence, Δi_{P2} is easily understood to exhibit a maximum in 0.2 mol/L NaOH solution.

According to Fleming's rule, the charged particles move in the Lorentz force direction, i.e., in a circular motion, which is perpendicular to the direction of magnetic induction [35]. Hence, the oxidation products are expected to relocate into a ring-like shape on the glassy alloy matrix. Under a magnetic field, the covered region Rc is more smooth than in the absence of a magnetic field, indicating an uneven variation under an applied magnetic field; this behavior has also been reported by Lu *et al.* [23]. The variation of regions Rb and Rc under a magnetic field are likely responsible for their contributions to the change in current density. As shown in Fig. 3(c), the current density i_{P2} increases slowly with increasing NaOH concentration in type II curves, i.e., in high-concentration NaOH solutions. Hence, the negative contribution to i_{P2} by the cleaner Rc under the magnetic field is greater than the positive contribution by the more severely corroded Rb. Therefore, Δi_{P2} is expected to be negative in the type II curves, which explains the non-monotonic variation of Δi_{P2} in the measured NaOH concentration range.

(2) In NaCl solutions. Similar to anodic polarization in NaOH solutions in Fig. 3, the anodic current density i_{Z2} of type I′ curves in NaCl solutions increases under an applied 0.02-T magnetic field (as shown in Fig. 6). This result indicates that chloride ions in the low-concentration NaCl solu-

tions pass the oxidation film more easily in the presence of a magnetic field, which can be explained by the MHD effect [39] and by the arguments of Lu *et al.* [22]. In 0.05 mol/L NaCl solution, the tubers on the corroded glassy alloy surface become stepped pits under the magnetic field, the size of which are larger than those formed in the absence of a magnetic field (as shown in Fig. 7). The corroded morphology also indicates that the mass transport is strengthened by the introduction of a magnetic field.

In the case of type II′ curves, the sufficient chloride ions are present in the NaCl solution and the oxidation reactions are fierce at the beginning of anodic dissolution. Under the magnetic field, Fe^{3+} and Cl^- ions are aggregated on the electrode; this aggregation can cause an increase in the viscosity of the electrolyte, and a maximum electrogeneration rate of molecules is possibly surpassed according to the arguments of Ragsdale *et al.* [39]. Hence, the current density i_{Z2} decreases under the 0.02-T magnetic field, which is consistent with the variation of i_{P2} in NaOH solutions.

5. Conclusions

(1) The current density prepeak PP in the anodic polarization curves in low-concentration NaOH solutions (classified as type I) tends to disappear when the NaOH concentration is increased to 0.4 mol/L as well as when the magnetic field is applied.

(2) The magnetic field exerts a non-monotonic effect on the anodic current density of $Fe_{78}Si_9B_{13}$ glassy alloy in both NaOH and NaCl solutions.

(3) The magnetic field can cause ring-like patterns and round pits on the alloy surface, and some of the effects of the magnetic field are explained by the MHD effect.

Acknowledgements

This work was financially supported by the National Natural Science Foundation of China (No. 51171091), the Excellent Youth Project of Shandong Natural Science Foundation (No. JQ201012), and the Major State Basic Research Development Program of China (No. 2012CB825702).

References

[1] A. Inoue, T. Zhang, and T. Masumoto, Zr–Al–Ni amorphous alloys with high glass transition temperature and significant supercooled liquid region, *Mater. Trans. JIM*, 31(1990), No. 3, p. 177.

[2] M. Tenhover, W.L. Johnson, and C.C. Tsuei, Upper critical fields of amorphous transition metal based alloys, *Solid State Commun.*, 38(1981), p. 53.

[3] C.L. Qin, W. Zhang, K. Asami, N. Ohtsu, and A. Inoue, Glass formation, corrosion behavior and mechanical properties of bulk glassy Cu–Hf–Ti–Nb alloys, *Acta Mater.*, 53(2005), p. 3903.

[4] Y.X. Geng, Y.M. Wang, J.B. Qiang, Q. Wang, F.Y. Kong, G.F. Zhang, and C. Dong, Formation and properties of high Fe-content Fe–(B–Si)–Zr bulk amorphous alloys, *Int. J. Miner. Metall. Mater.*, 20(2013), No. 4, p. 371.

[5] H.X. Li, S.L. Wang, Y. Jeong, and S. Yi, Corrosion behaviors of thermally grown oxide films on Fe-based bulk metallic glasses, *Int. J. Miner. Metall. Mater.*, 19(2012), No. 8, p. 726.

[6] X.G. Yang, K. Eckert, S. Mühlenhoff, and S. Odenbach, On the decay of the Lorentz-force-driven convection in vertical concentration stratification during magnetoelectrolysis, *Electrochim. Acta*, 54(2009), p. 7056.

[7] W.J. Lorentz and K.E. Heusler, *Anodic Dissolution of Iron Group Metal*, F. Mansfeld ed., Marcel Dekker, New York, 1987, p. 1.

[8] T.Z. Fahidy, Magnetoelectrolysis, *J. Appl. Electrochem.*, 13(1983), p. 553.

[9] C. Wang, S.H. Chen , X.G. Yang, and L. Li, Investigation of chloride-induced pitting processes of iron in the H_2SO_4 solution by the digital holography, *Electrochem. Commun.*, 6(2004), p. 1009.

[10] X.G. Yang, S.H. Chen, C. Wang, and L. Li, In-line digital holography for the study of dynamic processes of electrochemical reaction, *Electrochem. Commun.*, 6(2004), p. 643.

[11] X.G. Yang, S.H. Chen, L. Li, and C. Wang, Digital holographic study of the effect of magnetic field on the potentiostatic current oscillations of iron in sulfuric acid, *J. Electroanal. Chem.*, 586(2006), p. 173.

[12] L. Li, C. Wang, S.H. Chen, X.G. Yang, B.Y. Yuan, and H.L. Jia, An investigation on general corrosion and pitting of iron with the in-line digital holography, *Electrochim. Acta*, 53(2008), p. 3109.

[13] B.Y. Yuan, S.H. Chen, X.G. Yang, C. Wang, and L. Li, Mapping the transient concentration field within the diffusion layer by use of the digital holographic reconstruction, *Electrochem. Commun.*, 10(2008), p. 392.

[14] J.A. Koza, S. Mühlenhoff, M. Uhlemann, K. Eckert, A. Gebert, and L. Schultz, Desorption of hydrogen from an electrode surface under influence of an external magnetic field: *in-situ* microscopic observations, *Electrochem. Commun.*, 11(2009), p. 425.

[15] R. Sueptitz, K. Tschulik, M. Uhlemann, L. Schultz, and A. Gebert, Effect of high gradient magnetic fields on the anodic behavior and localized corrosion of iron in sulphuric acid solutions, *Corros. Sci.*, 53(2011), p. 3222.

[16] R. Sueptitz, J. Koza, M. Uhlemann, A. Gebert, and L. Schultz, Magnetic field effect on the anodic behavior of a ferromagnetic electrode in acidic solutions, *Electrochim. Acta*, 54(2009), p. 2229.

[17] A. Krause, J. Koza, A. Ispas, M. Uhlemann, A. Gebert, and A. Bund, Magnetic field induced micro-convective phenomena inside the diffusion layer during the electrodeposition of Co, Ni and Cu, *Electrochim. Acta*, 52(2007), p. 6338.

[18] V.C. Noninski, Magnetic field effect on copper electrodeposition in the Tafel potential region, *Electrochim. Acta*, 42(1997), p. 251.

[19] J. Lee, S.R. Ragsdale, X.P. Gao, and H.S. White, Magnetic field control of the potential distribution and current at microdisk electrodes, *J. Electroanal. Chem.*, 422(1997), p. 169.

[20] J.A. Koza, S. Mühlenhoff, P. Żabiński, P.A. Nikrityuk, K. Eckert, M. Uhlemann, A. Gebert, T. Weier, L. Schultz, and S. Odenbach, Hydrogen evolution under the influence of a magnetic field, *Electrochim. Acta*, 56(2011), p. 2665.

[21] J.A. Koza, M. Uhlemann, A. Gebert, and L. Schultz, The effect of a magnetic field on the pH value in front of the electrode surface during the electrodeposition of Co, Fe and CoFe alloys, *J. Electroanal. Chem.*, 617(2008), p. 194.

[22] Z.P. Lu, C.B. Huang, D.L. Huang, and W. Yang, Effects of a magnetic field on the anodic dissolution, passivation and transpassivation behavior of iron in weakly alkaline solutions with or without halides, *Corros. Sci.*, 48(2006), p. 3049.

[23] Z.P. Lu, D.L. Huang, W. Yang, and J. Congleton, Effects of an applied magnetic field on the dissolution and passivation of iron in sulphuric acid, *Corros. Sci.*, 45(2003), p. 2233.

[24] A. Gebert, V. Haehnel, E.S. Park, D.H. Kim, and L. Schultz, Corrosion behavior of $Mg_{65}Cu_{7.5}Ni_{7.5}Ag_5Zn_5Gd_5Y_5$ bulk metallic glass in aqueous environments, *Electrochim. Acta*, 53(2008), p. 3403.

[25] H.B. Lu, L.C. Zhang, A. Gebert, and L. Schultz, Pitting corrosion of Cu–Zr metallic glasses in hydrochloric acid solutions, *J. Alloys Compd.*, 462(2008), p. 60.

[26] Z.P. Lu, T. Shoji, and W. Yang, Anomalous surface morphology of iron generated after anodic dissolution under magnetic fields, *Corros. Sci.*, 52(2010), p. 2680.

[27] M. Keddam, *Corrosion Mechanisms in Theory and Practice, Seconded*, P. Marcus ed., Marcel DekkerInc, New York, 2002, p. 97.

[28] C.N. Cao, *Principles of Electrochemistry of Corrosion* (I), Chemical Industry Press, Beijing, 1985, p. 7.

[29] X.D. Bai, *Corrosion and Control of Materials*, Tsinghua University Press, Beijing, 2005, p. 36.

[30] A. Lekatou, A. Marinou, P. Patsalas, and M.A. Karakassides, Aqueous corrosion behavior of Fe–Ni–B metal glasses, *J. Alloys Compd.*, 483(2009), p. 514.

[31] A. Baton, D. Szewieczek, and G. Nawrat, Corrosion of amorphous and nanocrystalline Fe-based alloys and its influence on their magnetic behavior, *Electrochim. Acta*, 52(2007), p. 5690.

[32] G.H. Li, S.P. Pan, J.Y. Qin, Z.H. Zhang, and W.M. Wang, Insight into thermodynamics and corrosion behavior of Al–Ni–Gd glassy alloys from atomic structure, *Corros. Sci.*, 66(2013), p. 360.

[33] S. Hiromoto, A.P. Tsai, M. Sumita, and T. Hanawa, Effect of chloride ion on the anodic polarization behavior of the $Zr_{65}Al_{7.5}Ni_{10}Cu_{17.5}$ amorphous alloy in phosphate buffered solution, *Corros. Sci.*, 42(2000), No. 9, p. 1651.

[34] Z.P. Lu and W. Yang, *In situ* monitoring the effects of a magnetic field on the open-circuit corrosion states of iron in acidic and neutral solutions, *Corros. Sci.*, 50(2008), p. 510.

[35] X.G. Yang, K. Eckert, and S. Odenbach, Oscillatory Lorentz-force-driven flows during potentiostatic current oscillations in magnetic fields, *Electrochem. Commun.*, 12(2010), p. 1576.

[36] O. Aaboubi, J.P. Chopart, J. Douglade, A. Olivier, C. Gabrielli, and B. Tribollet, Magnetic field effects on mass transport, *J. Electrochem. Soc.*, 137(1990), p. 1796.

[37] R.A. Tacken and L.J.J. Janssen, Applications of magnetoelectrolysis, *J. Appl. Electrochem.*, 25(1995), p. 1.

[38] Y. Saito, A theoretical study on the diffusion current at the stationary electrodes of circular and narrow band types, *Rev Polarogr.*, 15(1968), No. 6, p. 177.

[39] S.R. Ragsdale, K.M. Grant, and H.S. White, Electrochemically generated magnetic forces: enhanced transport of a paramagnetic redox species in large, nonuniform magnetic fields, *J. Am. Chem. Soc.*, 120(1998), p. 13461.

[40] R.A. Malmsten, C.P. Smith, and H.S. White, Electrochemistry of concentrated organic redox solutions, *J. Electroanal. Chem.*, 215(1986), p. 223.

[41] S.C. Paulson, N.D. Okerlund, and H.S. White, Diffusion currents in concentrated redox solutions, *Anal. Chem.*, 68(1996), p. 581.